Phase Diagram Constructed from the HPLC Fractions of a Polystyrene-*b*-polyisoprene Prepared by Anionic Polymerization

Soojin Park, Kyoon Kwon, Donghyun Cho, Byeongdu Lee, Moonhor Ree, and Taihyun Chang*

Department of Chemistry and Polymer Research Institute, Pohang University of Science and Technology, Pohang 790-784, Korea

Received February 3, 2003

Introduction

Block copolymer systems have received continuing attention due to their self-assembled microdomain structure.[1,2] Depending on the interaction strength and the relative composition of the different blocks, block copolymers exhibit nanoscale phase separated morphology. The phase behavior of block copolymers has been extensively studied both theoretically and experimentally.[3−7] To construct a phase diagram of a block copolymer species, many samples of different compositions are needed.[4,7−10] It is nontrivial to acquire a good set of block copolymers for the purpose, and sometimes the samples of different compositions are mixed to make the wanted composition if appropriate samples are not available.[11,12]

Recently, we reported that block copolymers made by anionic polymerization can be fractionated by HPLC, and the composition variation of the HPLC fractions of a PS-*b*-PI diblock copolymer was large enough to exhibit different morphologies.[13] In the present study, we fractionated a PS-*b*-PI diblock copolymer by two-dimensional HPLC (2D-LC) and investigated their phase behavior by small-angle X-ray scattering (SAXS) and transmission electron microscopy (TEM). We could construct a detailed phase diagram of PS-*b*-PI over a ca. 10% composition range.

Experimental Section

Materials. A PS-*b*-PI diblock copolymer was synthesized by sequential anionic polymerization at 45 °C under an Ar atmosphere using *sec*-butyllithium (Aldrich) and cyclohexane (Aldrich) as an initiator and a solvent, respectively. Details of the apparatus and the polymerization procedure were reported previously.[14,15] The PS-*b*-PI was characterized by SEC and ^{1}H NMR (Bruker, DPX-300) to have $M_n = 34.0$ kg/mol, $M_w/M_n = 1.02$, and the PI content = 63.4 wt %. For the SEC analysis, two PS gel columns (Polymer Lab., PL-mixed C) were used, and the eluent was THF (Duksan, HPLC grade). The temperature of the column was 40 °C, and the chromatograms were recorded with a multiangle laser light scattering detector (Wyatt, mini-DAWN) and a refractive index detector (Wyatt, Opti-Lab).

HPLC Fractionation. Details of the 2D-LC procedure were reported previously.[13] The HPLC apparatus consists of a solvent delivery pump (Bischoff), a 10-port sample injector (Rheodyne, selectPro) equipped with a 100 μL injection loop, and a UV/vis absorption detector (Spectra-Physics) operated at 260 nm. For the reversed phase LC fractionation, a C18 bonded silica column (Nucleosil, 100 Å pore, 70 × 22 mm) and a mobile phase of CH_2Cl_2/CH_3CN mixture (80/20, v/v) were used. The injection sample concentration was 140 mg/mL, and the flow rate of the mobile phase was 1.5 mL/min. For the normal phase LC fractionation, a diol-bonded silica column (Nucleosil, 100 Å pore, 100 mm × 22 mm) and a mixture of isooctane/THF (75/25, v/v) were used. HPLC grade CH_2Cl_2 (Duksan), CH_3CN (Duksan), isooctane (Mallinckrodt), and THF (Duksan) were used. The mother PS-*b*-PI was fractionated into three fractions each by reversed and normal phase LC to result in nine fractions differing in PI and PS block lengths, respectively. An autoinjector (homemade) and an autocollector (Foxy Jr., LabAlliance) were used to facilitate the fractionation. The nine fractions were characterized by SEC and ^{1}H NMR, and the results are summarized in Table 1.

Small-Angle X-ray Scattering (SAXS). SAXS measurements were carried out at the synchrotron SAXS facility in the Pohang Light Source, Korea.[16] The wavelength (λ) of the X-ray beam was 1.608 Å, and the energy resolution ($\Delta\lambda/\lambda$) was 1.5×10^{-2}. PS-*b*-PI specimens contain 0.3 wt % 2,6-di-*tert*-butyl-4-methylphenol. The antioxidant was added to the toluene solution of the polymers, and the solvent was slowly evaporated for 1 day at room temperature and further evaporated under vacuum at 50 °C for 1 day. Then the polymer samples were annealed in the 1 mm thick spacer at 120 °C for 24 h under vacuum and cooled to room temperature. SAXS profiles were obtained at room temperature first and then as heated at a heating rate of 2 °C/min. Thus, the obtained SAXS intensity was corrected for absorption and air scattering.

Transmission Electron Microscopy (TEM). Transmission electron micrographs were obtained to identify the morphology of the samples annealed at 120 °C for 24 h. Electron transparent films of the mother and the fractionated PS-*b*-PI were cryo-microtomed (RMC Ultracut) to a nominal thickness of 50−80 nm at −120 °C and transferred to Cu grids. The specimens were stained by exposure for 1 h to OsO_4 (Polysciences, 0.4% in water) vapor before taking bright-field TEM (Hitachi-7600) micrographs.

Results and Discussion

Morphology of the Mother and Fractionated PS-*b*-PI. Figure 1 displays the SAXS profiles of the mother PS-*b*-PI and its nine fractions measured at room temperature. The SAXS profiles are presented in a log I vs q plot, in which I is the scattering intensity and q is the magnitude of the scattering wave vector, $q = (4\pi/\lambda)\sin(\theta/2)$. The morphology of block copolymers is sometimes difficult to be determined by the SAXS profile only. For example, the mother PS-*b*-PI has hexagonally perforated layer (HPL) morphology. The spacing of the perforated layers is 25.1 nm, which is smaller than that of the layer spacing (27.3 nm) of the S_HI_M sample having similar molecular weights but a lamellar morphology. The SAXS pattern of a shear aligned sample with HPL morphology exhibits a few diffraction peaks near the first-order diffraction (q^*) in addition to the integral multiple q^* positions due to the layer structure.[17] It is often hard for a nonaligned sample to observe the conspicuous peaks near q^*, and a broad peak is observed for the mother PS-*b*-PI. Therefore, the morphology of the sample needs to be confirmed by TEM. A TEM micrograph of the mother PS-*b*-PI is shown in Figure 2. In the TEM micrograph, the PI phase appears dark since OsO_4 preferentially stains the double bonds in the PI block. The TEM picture shows the dark PI lamellae are perforated by the light PS domain.

The SAXS profiles of S_HI_L, S_MI_L, and S_HI_M in Figure 1 show scattering maxima at the integral multiples of q^*, which clearly reflect the lamellar (LAM) morphology with domain periodicities of about 27 nm. The LAM morphology of S_HI_L is clearly confirmed from the TEM micrograph shown in Figure 2. S_LI_L and S_MI_M fractions

* Corresponding author: Tel +82-54-279-2109; FAX +82-54-279-3399; e-mail tc@postech.edu.

10.1021/ma030086r CCC: $25.00
Published on Web 05/20/2003

Table 1. Molecular Characteristics and Phase Behavior of the PS-*b*-PI Block Copolymers[a]

Mother PS-b-PI (M_n = 34.0 kg/mol, f_{PI} = 0.665, HPL $\xrightarrow{170°C}$ G $\xrightarrow{230°C}$ Dis)				
Sample Code[b]		NPLC		
		S_L	S_M	S_H
RPLC	I_H	33.2 kg/mol[c] 0.706[d] HEX $\xrightarrow{200°C}$ Dis[e]	34.8 kg/mol 0.687 G $\xrightarrow{170°C}$ HEX $\xrightarrow{210°C}$ Dis	35.0 kg/mol 0.672 G $\xrightarrow{205°C}$ HEX $\xrightarrow{230°C}$ Dis
	I_M	30.8 kg/mol 0.675 G $\xrightarrow{180°C}$ HEX $\xrightarrow{210°C}$ Dis	32.7 kg/mol 0.657 HPL $\xrightarrow{165°C}$ G $\xrightarrow{220°C}$ Dis	34.3 kg/mol 0.637 LAM $\xrightarrow{165°C}$ HPL $\xrightarrow{190°C}$ G $\xrightarrow{240°C}$ Dis
	I_L	30.6 kg/mol 0.638 HPL $\xrightarrow{165°C}$ G $\xrightarrow{245°C}$ Dis	31.2 kg/mol 0.627 LAM $\xrightarrow{190°C}$ G $\xrightarrow{230°C}$ Dis	32.4 kg/mol 0.608 LAM $\xrightarrow{245°C}$ Dis

[a] Transition temperatures are measured by SAXS at a heating rate of 2 °C/min. [b] S and I stand for PS and PI block fractionated by 2D-LC. Subscripts L, M, and H stand for low, medium, and high molecular weight fractions, respectively. [c] Number-average molecular weight determined by SEC−light scattering. [d] Volume fraction of PI block determined by ^{1}H NMR spectroscopy. [e] LAM = lamellae, HPL = hexagonally perforated layers, G = gyroids, HEX = hexagonal cylinders, Dis = disordered phase.

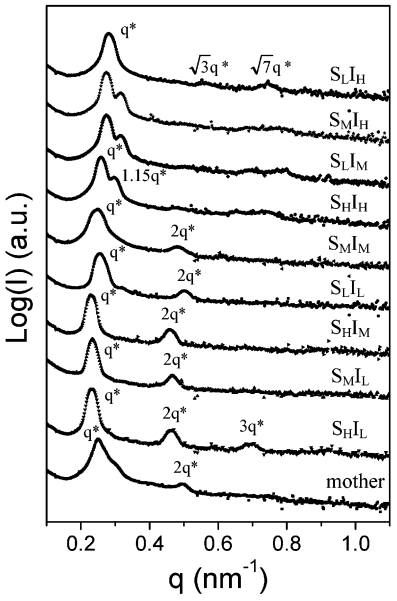

Figure 1. SAXS profiles of mother PS-*b*-PI and the fractions annealed at 120 °C. It is apparent that they show a variety of morphologies.

show SAXS profiles analogous to that of the mother PS-*b*-PI, showing a broad q^* peak and the peaks at the integral multiple q^* in Figure 1. The HPL morphology of S_MI_M is confirmed in the TEM image in Figure 2. It shows a very clear TEM image of a well-aligned single grain likely due to the narrower molecular weight and composition distribution of S_MI_M than the mother PS-*b*-PI.

The SAXS profiles of S_HI_H, S_LI_M, and S_MI_H samples in Figure 1 correspond to gyroid (G) morphology, which exhibit two distinct diffraction peaks at q^* and $1.15q^*$ and a number of weak higher-order reflections. The TEM micrograph of S_LI_M in Figure 2 shows the G microdomain structure with 3-fold symmetry. The S_LI_H sample in Figure 1 is easily categorized to the hexagonal cylinder (HEX) structure. The higher-order scattering peaks appearing at the scattering vectors of $\sqrt{3}q^*$ and $\sqrt{7}q^*$ are clear. The $\sqrt{4}q^*$ peak is extinct at the composition of S_LI_H.[18] The HEX morphology of S_LI_H sample is confirmed by TEM, as shown in Figure 2.

Phase Diagram from SAXS Measurements. The phase behavior (OOTs and ODTs) of block copolymer systems has been studied by various techniques such as SAXS, rheology, birefringence, etc.[7,19−23] We used SAXS to investigate the phase behavior. Figure 3A shows the SAXS profiles of the S_HI_M sample at different temperatures, which exhibit two OOTs and an ODT. The SAXS profiles obtained over a temperature range from 120 to 160 °C in Figure 1 show LAM phases as signified by the scattering peaks appearing at the integral multiples of q^*. The $OOT_{LAM-HPL}$ takes place near 165 °C, at which the first-order scattering peak begins to broaden due to the appearance of shoulders at both sides of the first-order scattering peak.[17] The two shoulder peaks become conspicuous at 180 °C. The $OOT_{LAM-HPL}$ temperature can be determined clearly by a discontinuity in the plot of the reciprocal of the first-order peak maximum intensity ($1/I_m$) vs the reciprocal of the absolute temperature ($1/T$) (filled square) in Figure 3B. Also, $OOT_{LAM-HPL}$ accompanies a sharp drop of the domain spacing ($D = 2\pi/q^*$) due to the perforation of the PS block (open triangle).

The microdomain structure changes again from HPL to G at near 190 °C as indicated by the shape change of the first scattering peak shape and the appearance of the two peaks at q^* and $1.15q^*$ in Figure 3A. The peak at $1.15\ q^*$ becomes distinct in the SAXS profiles taken at 220 and 235 °C. While the OOT_{HPL-G} does not show a clear signature in the domain spacing, the maximum scattering intensity changes significantly, and the OOT_{HPL-G} is clearly observed in the $1/I_m$ vs $1/T$ plot, as

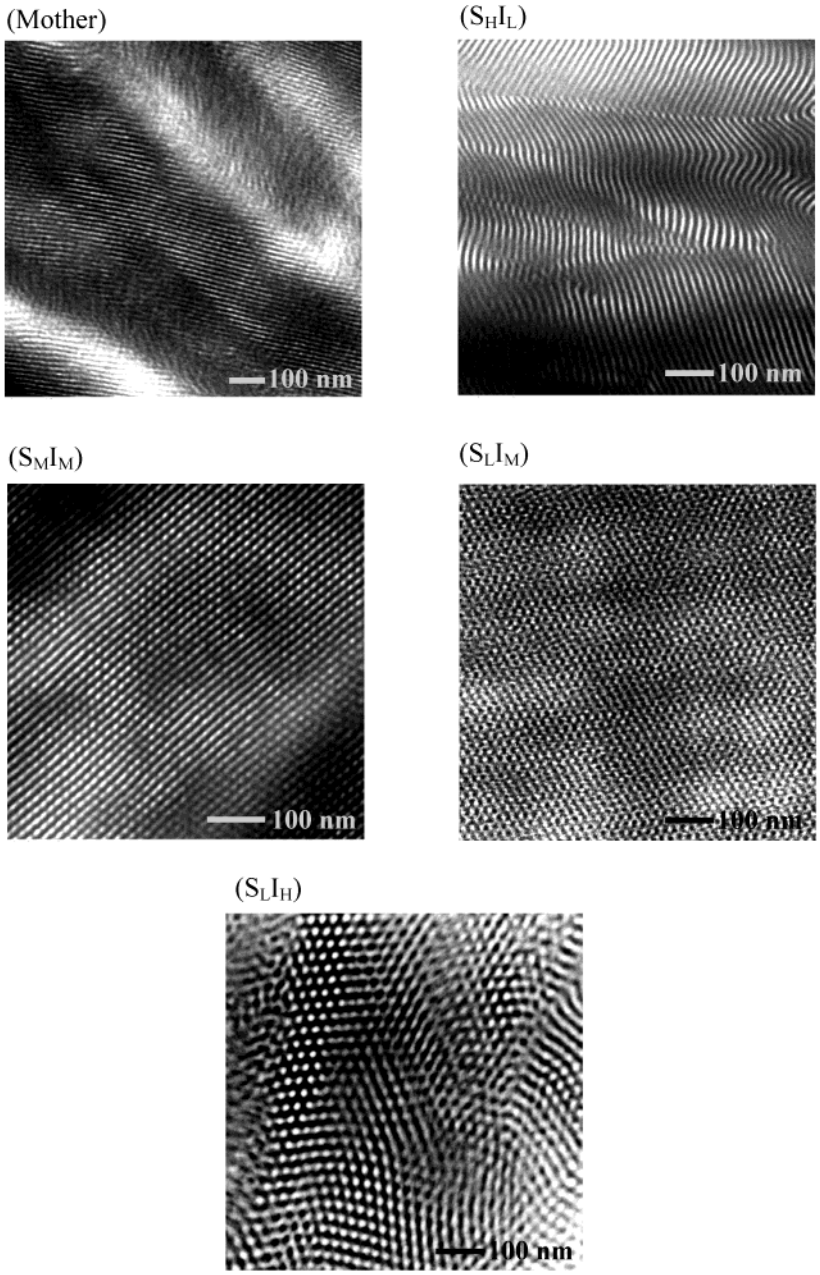

Figure 2. TEM micrographs of the mother PS-*b*-PI and its HPLC fractions. The HPLC fractions show very clear morphology; in particular, a well-developed HPL microdomain structure was observed for S_MI_M even though this sample was not shear aligned.

shown in Figure 3B. Finally, the ODT takes place at 240 °C where the maximum scattering intensity decreases sharply. In this way we could measure the OOT and ODT temperatures of the mother PS-*b*-PI and the nine fractions. The results are summarized in Table 1, and a detailed phase diagram of χN vs PI volume fraction (f_{PI}) was constructed, as displayed in Figure 4. We assumed that the interaction parameter $\chi = -0.0419 + 38.54/T$ for PS-*b*-PI, independent of composition and molecular weight.[24] Also, N and f_{PI} are calculated according to the following formulas after Helfand[25]

$$N = (\rho_{PS}\rho_{PI})^{1/2}(N_{PS}/\rho_{PS} + N_{PI}/\rho_{PI}) \quad (1)$$

$$f_{PI} = (N_{PI}/\rho_{PI})/[(N_{PS}/\rho_{PS} + N_{PI}/\rho_{PI})] \quad (2)$$

where N_{PS} and N_{PI} are the number-average degree of polymerization of PS and PI blocks and ρ_{PS} and ρ_{PI} are segmental densities of PS and PI, respectively; $\rho_{PS} = 1.01 \times 10^4$ mol/m^3 and $\rho_{PI} = 1.34 \times 10^4$ mol/m^3.

In Figure 4, the squares, circles, triangles, and stars stand for LAM, HPL, G, and HEX morphology found in the SAXS measurements, respectively. The rhombuses are ODT points, and the filled symbols represent the mother PS-*b*-PI. The points in one vertical line (a constant f_{PI}) represent the data set for a PS-*b*-PI sample measured at different temperatures. Therefore, there are 10 lines for the nine fractions and the mother PS-*b*-PI, covering about 10% in the PI volume fraction. The dotted line is the mean-field prediction of the ODT. We also investigated the long-term stability of the HPL phase as follows. First, the HPLC fractions showing the HPL morphology (mother, S_LI_L, S_MI_M, and S_HI_M) were annealed at 160 °C (below $OOT_{HPL\rightarrow G}$) for 8 days. They are shown as left-half filled circles in Figure 4. After the annealing, all the samples were transformed to G

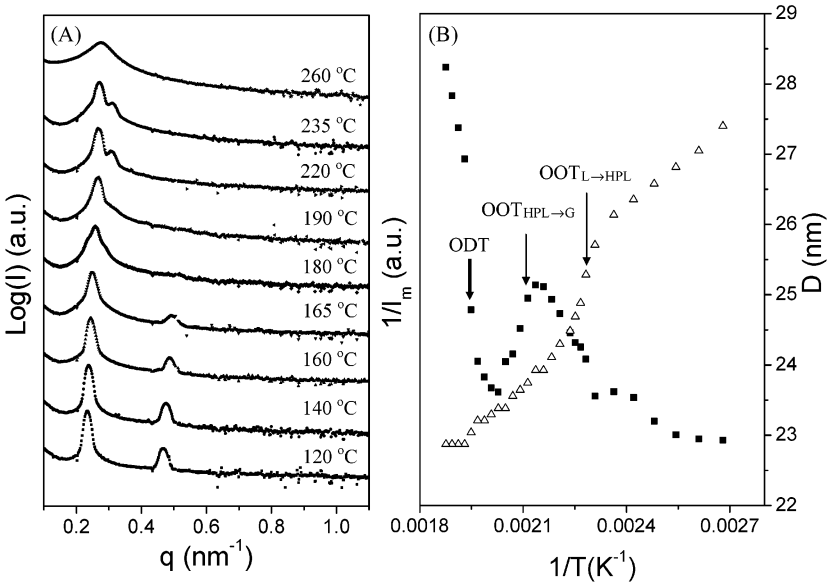

Figure 3. SAXS profiles of the S_HI_M sample at different temperatures (A) and the plot of reciprocal of the maximum scattering intensity (filled square) and the domain spacing (open triangle) vs $1/T$ (B). The OOT and ODT can be determined from the abrupt change(s) in these plots. The OOT_{L-HPL}, OOT_{HPL-G}, and ODT are marked with arrows in (B).

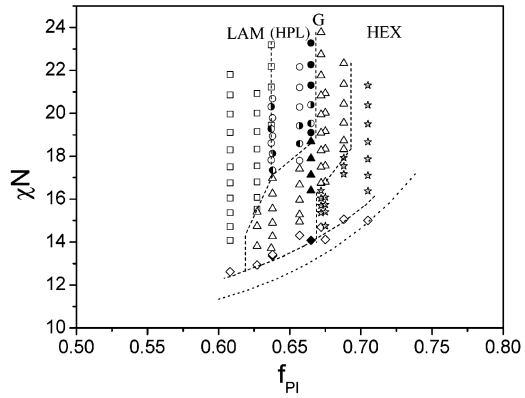

Figure 4. Phase diagram of PS-*b*-PI constructed with the fractionated PS-*b*-PIs. Different symbols stand for the different morphology as shown in the figure. Filled symbols represent the mother PS-*b*-PI. The dotted line is the ODT calculated according to the mean filed theory while rhombuses are the measured ODT. The dashed line is the phase boundary drawn for visual aid. Half-filled circles represent the data points to test the stability of HPL phase. Refer to the text for details.

phases. Second, we annealed the samples for 24 h at 190 °C to ensure G morphology. Then the samples were slowly cooled to 150 °C and annealed at 150 °C for 7 days. All the fractions maintained G morphology at 150 °C, and the right half-filled circles in Figure 4 represent the experimental results. From the results of the two different experiments, we can conclude that the HPL phase is not a stable equilibrium phase although the HPL morphology was observed by SAXS and TEM during the heating process. Therefore, we speculate that the area labeled by HPL would belong to G in the long run and label the area as (HPL) in a bracket.

The general feature of this phase diagram is similar to the results of Khandpur et al. on PS-*b*-PI diblock copolymers.[9] However, it shows the very fine details of the phase behavior near ODT over the narrow composition range, which would not be easy to be obtained without such a well-defined set of the polymer samples of the similar molecular weights and compositions. The phase behavior of the mother PS-*b*-PI including OOT and ODT points is not much distinguishable from the fractions, and the metastability of HPL phase is also not much different from the unfractionated samples. However, the TEM image shows a much clearer HPL structure for the S_MI_M fraction than the mother PS-*b*-PI. The large grain size of the S_MI_M fraction is likely due to the narrower distribution in molecular weight and composition. However, it would be too early to reach a conclusion, and a more systematic effort is called for to clarify the issue on how the polydispersity affects the phase behavior of block copolymers.

In summary, by 2D-LC we fractionated a mother PS-*b*-PI diblock copolymer prepared by anionic polymerization into nine fractions differing in the PI and PS block lengths. In this way we could obtain PS-*b*-PIs of the similar molecular weight (<15% variation). The fractions show composition variation large enough to construct a detailed phase diagram over ca. 10% composition range. By virtue of the narrower distributions in both molecular weight and composition of the fractions, we could observe sharper OOT phase boundaries and better-defined morphologies as observed by SAXS and TEM.

Acknowledgment. This paper is dedicated to Prof. Won-Jei Cho on the occasion of his retirement. This study was in part supported by KOSEF (Center for Integrated Molecular Systems), the BK 21 program, and the Pohang Accelerator Laboratory. We thank Mr. Jehan Kim for his help in the synchrotron SAXS measurements at PAL.

References and Notes

(1) Bates, F. S.; Fredrickson, G. H. *Annu. Rev. Phys. Chem.* **1990**, *41*, 525.
(2) Hamley, I. W. *The Physics of Block Copolymers*; Oxford University Press: New York, 1998.
(3) Leibler, L. *Macromolecules* **1980**, *13*, 1602.
(4) Bates, F. S.; Schulz, M. F.; Khandpur, A. K.; Förster, S.; Rosedale, J. H. *Faraday Discuss.* **1994**, *98*, 7.
(5) Matsen, M. W.; Schick, M. *Macromolecules* **1994**, *27*, 4014.
(6) Hashimoto, T. *Macromol. Symp.* **2001**, *174*, 69.
(7) Lodge, T. P.; Pudil, B.; Hanley, K. J. *Macromolecules* **2002**, *35*, 4707.

(8) Förster, S.; Khandpur, A. K.; Zhao, J.; Bates, F. S.; Hamley, I. W.; Ryan, A. J.; Bras, W. *Macromolecules* **1994**, *27*, 6922.
(9) Khandpur, A. K.; Förster, S.; Bates, F. S.; Hamley, I. W.; Ryan, A. J.; Bras, W.; Almdal, K.; Mortensen, K. *Macromolecules* **1995**, *28*, 8796.
(10) Floudas, G.; Vazaiou, B.; Schipper, F.; Ulrich, R.; Wiesner, U.; Iatrou, H.; Hadjichristidis, N. *Macromolecules* **2001**, *34*, 2947.
(11) Hajduk, D. A.; Harper, P. E.; Gruner, S. M.; Honeker, C. C.; Kim, G.; Thomas, E. L.; Fetters, L. J. *Macromolecules* **1994**, *27*, 4063.
(12) Bodycomb, J.; Yamaguchi, D.; Hashimoto, T. *Macromolecules* **2000**, *33*, 5187.
(13) Park, S.; Cho, D.; Ryu, J.; Kwon, K.; Lee, W.; Chang, T. *Macromolecules* **2002**, *35*, 5974.
(14) Kwon, K.; Lee, W.; Cho, D.; Chang, T. *Korea Polym. J.* **1999**, *7*, 321.
(15) Lee, W.; Cho, D.; Chang, T.; Hanley, K. J.; Lodge, T. P. *Macromolecules* **2001**, *34*, 2353.
(16) Bolze, J.; Kim, J.; Huang, J. Y.; Rah, S.; Youn, H. S.; Lee, B.; Shin, T. J.; Ree, M. *Macromol. Res.* **2002**, *10*, 2.
(17) Ahn, J.-H.; Zin, W.-C. *Macromolecules* **2000**, *33*, 641.
(18) Hashimoto, T.; Kawamura, T.; Harada, M.; Tanaka, H. *Macromolecules* **1994**, *27*, 3063.
(19) Rosedale, J. H.; Bates, F. S. *Macromolecules* **1990**, *23*, 2329.
(20) Almdal, K.; Koppi, K. A.; Bates, F. S.; Mortensen, K. *Macromolecules* **1992**, *25*, 1743.
(21) Balsara, N. P.; Perahia, D.; Safinya, C. R.; Tirrell, M.; Lodge, T. P. *Macromolecules* **1992**, *25*, 3896.
(22) Kim, J. K.; Lee, H. H.; Gu, Q.-J.; Chang, T.; Jeong, Y. H. *Macromolecules* **1998**, *31*, 4045.
(23) Park, M. J.; Char, K.; Kim, H. D.; Lee, C.-H.; Seong, B.-S.; Han, Y.-S. *Macromol. Res.* **2002**, *10*, 325.
(24) Hashimoto, T.; Ijichi, Y.; Fetters, L. J. *J. Chem. Phys.* **1988**, *89*, 2463.
(25) Helfand, E. *Polym. Sci. Technol.* **1974**, *4*, 141.

MA030086R